Article

Numerical Modelling and Dynamic Analysis of Ocean Towed Cable-array System under Munk Moment during Turning Maneuver

Dapeng Zhang[1], Bowen Zhao[2]*, Yang Yang[1], Keqiang Zhu[3,] and Haoyu Jiang[4]

[1] Ship and Maritime College, Guangdong Ocean University, 524088, Guangdong Zhanjiang China;

[2] Department of Applied Mathematics and Mathematical Modeling, Saint-Petersburg State Marine Technical University, 190121, Saint-Petersburg, Russia；

[3] Faculty of Maritime and Transportation, Ningbo University, 315211, Zhejiang Ningbo, China

[4] School of Electronics and Information Engineering, Guangdong Ocean University, 524088, Guangdong Zhanjiang, China

Abstract: The ocean towing system plays an important role in the ocean development process. The motion of a towed body is closely coupled with the motion of a towing cable. Munk moment coefficient represents the value of Munk moment which is caused by axial flow. Munk moment seriously affects the motion stability of towed body. In this paper, reference to the parameters of a towed body and by using the lumped mass method, the dynamic simulation of a towed cable-array system in single 360° large-radius ship turn has been established by OrcaFlex. With the change of different Munk coefficients, the effect of real-time response of cable tension and towed body underwater con-figuration have been researched. The results show that Munk moment seriously affects the tension and curvature of the towed cable, especially the section close to the towed body. The larger the Munk moment, the larger the maximum value of the cable tension. This means that the ultimate tension on the cable is also larger. The results provide a theoretical basis for the optimal design of the towed cable and towed body.

Keywords: Cable-array system; Dynamic response; Turning maneuver; Munk moment; Lumped mass method

1. Introduction

With the development of marine science and technology, ocean towed system is playing a more and more important role in many fields, such as ocean monitoring, military detection, seabed mapping and naval defense [1,2]. In many types of applications, the systems include the towing ship, towed cable and towed body. Normally, the towed body is equipped with many types of oceans detecting instruments. The operation of instruments in towed system requires that the towed body should be stable during a towing operation. But under real ocean environments, the unsteady motion of a towing ship is transmitted down the cable to the towed body, resulting in perturbations both of attitude and position relative to the towing ship. Depending on the sea state and the response of a towing ship, these perturbations can be sufficiently large to throw off the towed body beyond acceptable limits. To maintain the attitude of a towed body as stable as possible under different towing conditions is one of the major concerns of users[3,4].

The study of hydrodynamic characteristics plays an important role in the preliminary design of the underwater towed system [5-7]. At present, researchers have done a lot of beneficial exploration and research on the hydrodynamic characteristics of the ocean towed cable-array system. The experiment and the numerical calculation are two main methods to study the motion of ocean towed cable-array system. For example, Kishore et al. [8]investigated the loop maneuver of an underwater towed cable-array system. The case studies showed that reducing the towed speed during a loop could cause a fast relaxation in the towed point tension, which would lead to severe problems. Srivastava and Ganapathy [9] conducted an experimental study on the same towed cable-array system. The results showed that the effect of a change in loop radius, keeping the towed speed nearly constant, was basically felt on the lateral shift of the array. As the loop radius was increased, the lateral shift of the array decreased. Gobat and Grosenbaugh [10] described a computer program for analyzing the statics and dynamics of a towed cable-array system. The program used the generalized-α time integration algorithm, adaptive time stepping, and adaptive spatial gridding to produce accurate, stable solutions for dynamic problems. According to the study, the nonlinear of the towed cable-array system was strong under waves, currents and wind environments. Holmes et al. [11] developed a novel experimental method involving an autonomous underwater vehicle (AUV) with a towed hydrophone array. The flow noise was a primary concern for the stability of the array. Grosenbaugh [12] studied the dynamic behavior of a towed cable system. The towing ship changed from straight towing track to stable turning track with constant radius. The dynamics of a single 360° turn and a 180° U-turn were discussed in terms of the transients of the steady turning maneuver. The results

Eng. Solut. Mech. Mar. Struct. Infrastruct., 2024, Vol. 1. Issue 2

3 of 20

showed the return of the ship to a straight-tow course after a 180° U-turn would cause the vehicle to pull out of its turning maneuver more quickly than for the 360° turn. Wang and Sun [13] analyzed the damped oscillation of towed cable system in different spiral courses. An oscillatory motion of the towed vehicle was found in simulation of spiral towed courses. Feng et al. [14] proposed a new approach to design an ideal towed system. A code was written to assist in designing the towed system. The governing equation was solved using a 4th-order Runge-Kutta numerical method for stable cable. Carey et al. [15] developed an array to demonstrate, and quantify the performance characteristics of an autonomous-vehicle towed-array system. The towed stability of the system enabled the use of the synthetic Hankel transform to estimate the modal horizontal wave number spectrum and the identification of interface wave speeds at frequencies up to 1000 Hz. The system was shown to provide a unique measurement capability for directional noise measurement in shallow water environments. Du et al. [16] studied the influence of underwater vehicle flow field on the dynamic behavior of towed sonar cable array through numerical method. The results showed that the numerical method was reasonable, and the lateral deflection of the towed sonar cable array was related to the speeds and the motion modes of the underwater vehicle. The greater the speed of underwater vehicle, the smaller the distance between the end and the top of towed sonar cable-array. The linear motion and surfacing motion of underwater vehicle produced a lateral deflection of the towed cable array at the beginning, while the turning motions produced the yaw angle of the array. Zhang et al. [17] investigated the dynamic responses of a wave glider with a towed body. The effects of wave parameters were studied. The more severe the wave motion, the greater the average velocity and the higher the oscillation of heave motion and forward velocity of the towed body, which indicated that the marine environment had an obvious influence on the performance of the towed system. Yang et al. [18], Yuan et al. [19], and Holmes et al [20]. studied the motion responses of ocean towed cable-array system under complex environmental loads. The prediction of dynamic response of towed cable-array system becomes more and more difficult with the increase of load types. Previous studies have provided strong references for the further dynamic behavior exploration of the ocean towed cable-array system [22-24].

With rapid development of computer technology, the simulations of complex fluid dynamics models become more and more convenient. Numerical calculation methods have been widely used in performance analysis of ocean towed cable-array system, which can be divided into three categories: finite element method, finite difference method and lumped mass method. The finite element method is widely used in engineering calculation. However, there will be more elements and nodes as the length of the flexible riser increases when it is

Eng. Solut. Mech. Mar. Struct. Infrastruct., 2024, Vol. 1, Issue 2

4 of 20

applied to the analysis of flexible risers. The increase of the number of elements and nodes will lead to the increase of the order of stiffness matrix, and the matrix will have great sparsity. Hence, it requires a large amount of calculation time and is not easy to achieve the convergence of the computation process. The finite difference method is also a numerical method for solving differential equations of subsea pipelines. It deals with differential equations, including ordinary differential equations and partial differential equations. The finite difference method requires a discrete approximation of the differential, which uses the function values of the surrounding points to approximate the differential of the point. The advantages of the finite difference method are intuitive and simple. However, it is not suitable for engineering problems with complex boundary conditions. Runge-Kutta method is a common numerical solution method, which is widely used in solving partial differential equations [24,25]. It is often combined with the lumped mass model to calculate the governing equations of the cable. The lumped mass method is a special form of finite element method. Different from the finite difference method which solves the governing equation from the point of view of micro-elements, the lumped mass method directly calculates from Newton's second law, approximating the cable as a series of nodes connected by massless linear elastic elements, and applying the distributed forces such as gravity and fluid dynamics on the distributed nodes of the cable [26-29]. Da Silva et al. [30] proposed a new discreet dynamic modeling formalism based on lumped mass method, in which both the tugboat and the towed vessel are subject to forces from waves on the sea surface. The continuous flexibility of the cable was approximated by a discrete equivalent, formed by rigid links connected by fictitious elastic joints that allowed elevation movements. Guo et al. [31] proposed a nonlinear numerical model to investigate the dynamic response characteristics of the towing cable. It was found that the proposed modeling applied to both high flexible cables and low flexible cables. Westin and Irani [32] presented a numerical method of a towed cable system based on the Absolute Nodal Coordinate Formulation. The simulated cable behavior was reliable compared to small scale experimental measurements. According to the literature, the lumped mass method is widely used in cable dynamic analysis for its clear physical meaning and easy-programming [33].

The towed body is modeled as a rigid body with six degrees of freedom, which is subjected to complex ocean environmental loads under water, such as current, turbulence, waves, etc. Munk moment refers to the couple of two equal and opposite forces generated by an object moving at a certain angle of attack (or drift) in a steady straight line in an ideal fluid on the front and rear halves. Munk moment may make the towed body unstable in simultaneous surge and sway motions [34,35]. Hakamifard and Rostami [36] calculated the

Eng. Solut. Mech. Mar. Struct. Infrastruct., 2024, Vol. 1. Issue 2

5 of 20

added mass coefficients for computation of Munk moment using analytical formulation in potential flow. The Munk moment of numerical simulation and analytical formulation was compared. The Munk moment seriously affects the motion stability of a towed body [37]. However, as can be seen from the brief review of the most advanced research, there are few studies on the influence of Munk moment on the hydrodynamic performance of ocean towed cable-array systems. Therefore, it is necessary to study the hydrodynamic response of ocean towing systems under Munk moment.

In this paper, the lumped mass method is used to discrete the towed cable into lumped mass model. At the same time, with the basis of some assumptions, the relationship between the expression of Munk moments in the classical towed body kinematics and the expression of Munk moments in the hydrodynamic analysis software OrcaFlex [38] is established. Based on the above derivation, combined with the specific parameters of a certain sea condition and towed cable system, the hydrodynamic response of the marine cable system under different Munk moment coefficients is modeled by OrcaFlex and its motion is calculated by time-domain coupled dynamic analysis method. The rest of this paper is organized as follows. Section 2 introduces the lumped mass method and the expression of Munk moment. Section 3 presents the numerical model and verifies the correctness and reliability of the lumped mass method. Section 4 presents the results and discussion. Finally, the conclusions drawn from this paper is presented in Section 5. The results provide a theoretical basis for the optimal design of the towed cable and towed body under the action of hydrodynamic moment.

2. Methodology

2.1 The lumped mass method

The towed cable model is seemed as a slender, flexible cylindrical cable. The discrete lumped mass model is used to solve the nonlinear boundary value problem. The basic idea of this model is to divide the towed cable into N segments, and the mass of each element is concentrated on one node, so that there are N+1 nodes. The tension $\boldsymbol{T}$ and shear $\boldsymbol{V}$ acting at the ends of each segment can be concentrated on a node, and any external hydrodynamic load is concentrated on the node. The motion equation of $\boldsymbol{i}$-th node ($\boldsymbol{i}$=0, 1…N) is [39,40]:

$$\boldsymbol{M}_{A_i}\ddot{\boldsymbol{R}}_i = \boldsymbol{T}_{e_i} - \boldsymbol{T}_{e_{i-1}} + \boldsymbol{F}_{dI_i} + \boldsymbol{V}_i - \boldsymbol{V}_{i-1} + \boldsymbol{w}_i\Delta\overline{s}_i \tag{1}$$

Among them, $\boldsymbol{R}$ represents the node position of the cable.

$\boldsymbol{M}_{Ai} = \Delta\overline{s}_i\left(m_i + \dfrac{\pi}{4}D_i^2(C_{an}-1)\right)\boldsymbol{I} - \Delta\overline{s}_i\dfrac{\pi}{4}D_i^2(C_{an}-1)(\tau_i \otimes \tau_{i-1})$ is the mass matrix of a node, $\boldsymbol{I}$ is the

3×3 identity matrix; $T_{ei} = EA\varepsilon_i = EA\dfrac{\Delta s_{0i}}{\Delta s_{\varepsilon i}}$, which stands for effective tension at a certain node;

$\Delta s_{0i} = L_0/(N-1)$, which represents the original length of each segment; $\Delta s_{\varepsilon i} = |R_{i+1} - R_i|$, the stretched length of each segment; *EA*, axial stiffness of the cable.

F_{dI_i} represents the external hydrodynamics [41] of each node, which is calculated according to the Morison equation:

$$M_{A_i}\ddot{R}_i = T_{e_i} - T_{e_{i-1}} + F_{dI_i} + V_i - V_{i-1} + w_i\Delta\overline{s}_i \qquad (2)$$

Where ρ is the density of sea water, D_i is the diameter of each cable, C_{dni} is the normal drag coefficient, C_{dti} is the tangential drag coefficient, C_{ani} is the inertia coefficient.

$$V_i = \frac{EI_{i+1}\tau_i \times (\tau_i \times \tau_{i+1})}{\Delta s_{\varepsilon i}\Delta s_{\varepsilon i+1}} - \frac{EI_i\tau_i \times (\tau_{i-1} \times \tau_i)}{\Delta s_{\varepsilon i}^2} + \frac{H_{i+1}\tau_i \times \tau_{i+1}}{\Delta s_{\varepsilon i}}$$, *V* represents the shear force at the node, *H* is the torsion.

2.2 Expression of Munk moments

2.2.1 Basic assumptions

Slender bodies in near-axial flow experience a destabilizing moment called the Munk moment. In order to derive the Munk moments, the following assumptions are made:

(1) The towed body is considered as a rigid body;

(2) The shape of the towed body is symmetric with respect to the *xOy* plane and the *xOz* plane. In the calculation of the additional mass, the asymmetry of the *xOz* plane that may be caused by the geometric shape of the towed body is ignored;

(3) the inertial product of the towed body is not taken into account, that means $J_{xy}=J_{yx}=J_{xz}=J_{zx}=J_{yz}=J_{zy}=0$;

(4) The towed body is completely submerged in the fluid medium and in a fully wet state;

(5) The change of the mass and mass distribution of the towed body in the course of navigation is negligible;

(6) Without considering the earth's autobiography and the curvature of the earth, the ground coordinate system is regarded as the inertial coordinate system.

2.2.2 Coordinate system

Inertial coordinate system $O_0x_0y_0z_0$, O_0 is the coordinate origin; *Oxyz* towed body coordinate system, $Ox_1y_1z_1$ velocity coordinate system, both for which the coordinate origin is taken at the center of buoyance *O*.

Eng. Solut. Mech. Mar. Struct. Infrastruct., 2024, Vol. 1. Issue 2

7 of 20

2.2.3 Definition of kinematic parameters

(1) Position coordinates and velocity:

$$r = \begin{bmatrix} x_0, y_0, z_0 \end{bmatrix}^T, \quad v = \begin{bmatrix} v_x, v_y, v_z \end{bmatrix}^T, \quad v_0 = \begin{bmatrix} v_{x0}, v_{y0}, v_{z0} \end{bmatrix}^T \tag{3}$$

(2) Attitude angle and angular velocity:

$$r = \begin{bmatrix} x_0, y_0, z_0 \end{bmatrix}^T, \quad v = \begin{bmatrix} v_x, v_y, v_z \end{bmatrix}^T, \quad v_0 = \begin{bmatrix} v_{x0}, v_{y0}, v_{z0} \end{bmatrix}^T \tag{4}$$

(3) Rudder angle and trajectory angle:

$$r = \begin{bmatrix} x_0, y_0, z_0 \end{bmatrix}^T, \quad v = \begin{bmatrix} v_x, v_y, v_z \end{bmatrix}^T, \quad v_0 = \begin{bmatrix} v_{x0}, v_{y0}, v_{z0} \end{bmatrix}^T \tag{5}$$

(4) Angle of attack α and sideslip angle β

Angle of attack α: the angle between the projection of the Ox_1 axis of the velocity coordinate system in the xOy plane of the towed body coordinate system and the Ox axis of the towed body coordinate system.

Sideslip angle β: the angle between the Ox_1 axis of the velocity coordinate system and the xOy plane of the towed body coordinate system.

2.2.4 Kinetic equation and kinematic equation

The equations of motion of the towed body includes kinetic equations and kinematic equations. The kinetic equation of the rigid body is used to describe the relationship between the force, acceleration and angular acceleration of the rigid body, the kinematic equations describe the dynamic relationship between the spatial position and the attitude and velocity and angular velocity.

According to the momentum theorem and the theorem of moment of momentum, the kinetic equation of the towed body can be obtained (The towed body has a small maneuver, the second order term of the moving parameter of the towed body is ignored, and the centroid position is the first order).

$$r = \begin{bmatrix} x_0, y_0, z_0 \end{bmatrix}^T, \quad v = \begin{bmatrix} v_x, v_y, v_z \end{bmatrix}^T, \quad v_0 = \begin{bmatrix} v_{x0}, v_{y0}, v_{z0} \end{bmatrix}^T \tag{6}$$

$$(m + \lambda_{22})\dot{v}_y + (mx_c + \lambda_{26})\dot{\omega}_z + mv_x\omega_z = \frac{1}{2}\rho v^2 S\left(C_y^\alpha \alpha + C_y^{\delta_e}\delta_e + C_y^{\bar{\omega}_z}\bar{\omega}_z\right) - \Delta G\cos\theta\cos\phi \tag{7}$$

$$(m + \lambda_{33})\dot{v}_z - (mx_c + \lambda_{35})\dot{\omega}_y - mv_x\omega_y = \frac{1}{2}\rho v^2 S\left(C_z^\beta \alpha + C_z^{\delta_r}\delta_r + C_z^{\bar{\omega}_y}\bar{\omega}_y\right) + \Delta G\cos\theta\sin\phi \tag{8}$$

$$(J_{xx} + \lambda_{44})\dot{\omega}_x - mv_x\left(y_c\omega_y + z_c\omega_z\right) = \frac{1}{2}\rho v^2 SL\left(m_x^\beta \beta + m_x^{\delta_r}\delta_r + m_x^{\delta_d}\delta_d + m_x^{\bar{\omega}_x}\bar{\omega}_x + \right.$$
$$\left. m_x^{\bar{\omega}_y}\bar{\omega}_y\right) + G\cos\theta\left(y_c\sin\phi + z_c\cos\phi\right) + \Delta M_{xp} \tag{9}$$

Eng. Solut. Mech. Mar. Struct. Infrastruct., 2024, Vol. 1. Issue 2

8 of 20

$$\left(J_{yy}+\lambda_{55}\right)\dot{\omega}_y-\left(mx_c-\lambda_{35}\right)\dot{v}_z+mx_cv_x\omega_y=\frac{1}{2}\rho v^2SL\left(m_y^\beta\beta+m_y^{\delta_r}\delta_r+m_y^{\bar{\omega}_x}\bar{\omega}_x+\right.$$
$$\left.m_y^{\bar{\omega}_y}\bar{\omega}_y\right)-G\left(x_c\cos\theta\sin\phi+z_c\sin\theta\right) \tag{10}$$

$$\left(J_{zz}+\lambda_{66}\right)\dot{\omega}_z+\left(mx_c+\lambda_{26}\right)\dot{v}_y+mx_cv_x\omega_z=\frac{1}{2}\rho v^2SL\left(m_z^\alpha\alpha+m_z^{\delta_e}\delta_e+m_z^{\bar{\omega}_z}\bar{\omega}_z\right)+$$
$$G\left(y_c\sin\theta-x_c\cos\theta\cos\phi\right) \tag{11}$$

Where m is the mass of towed body; λ is the added mass; $\dot{v}_x$, $\dot{v}_y$, $\dot{v}_z$, respectively, the acceleration of the towed body in m along the towed body coordinate system direction of x, y, z; T is the propulsive force; C_xS is the drag coefficient of the maximum cross section S as the characteristic area; ρ is the density of sea water; S is the maximum cross-sectional area; $\Delta G=G\text{-}B$, the negative buoyancy of the towed body; x_c, y_c, z_c, the centroid position coordinates; $\dot{\omega}_x$, $\dot{\omega}_y$, $\dot{\omega}_z$, respectively, angular accelerations along the x, y, z directions of the towed body in the towed body coordinate system; C_y^α, $C_y^{\delta_e}$, respectively, the derivative of the lift factor of the towed body with respect to the angle of attack α and the derivative of the position with respect to the horizontal rudder angle δ_e; C_z^β, $C_z^{\delta_r}$, respectively, the derivative of the side force factor with respect to the sideslip angle β and the derivative with respect to the vertical rudder angle δ_r; $C_y^{\bar{\omega}_z}$, the dimensionless factor of the lift force for the rotational derivative of the angular velocity ω_z; $C_y^{\bar{\omega}_y}$, the dimensionless factor of the lateral force for the rotational derivative of the angular velocity ω_y; $\bar{\omega}$, the dimensionless angular velocity ω; m_x^β, m_y^β, respectively, the position derivatives of the roll moment factor and yaw moment factor with respect to the sideslip angle β; m_z^α, the position derivative of the pitching moment factor of towed body with respect to the attack angle α; $m_x^{\delta_r}$, $m_x^{\delta_d}$, respectively, the position derivatives of the roll moment factor of the towed body with respect to the vertical rudder angle δ_r and the differential rudder angle δ_d; $m_y^{\delta_r}$, the derivative of the yaw moment factor with respect to the vertical rudder angle δ_r; $m_z^{\delta_e}$, the derivative of the pitching moment factor to the horizontal rudder angle δ_e; $m_x^{\bar{\omega}_x}$, $m_x^{\bar{\omega}_y}$, respectively, the rotational derivatives of the rolling moment factor with respect to ω_x and ω_y; $m_y^{\bar{\omega}_x}$, $m_y^{\bar{\omega}_y}$, respectively, the rotational derivatives of the yaw moment factor with respect to ω_x and ω_y; $m_z^{\bar{\omega}_z}$, the rotational derivative of the pitching moment factor with respect to ω_z; L, length of the towed body.

The kinematic equations describe the dynamic relationship between the spatial position, the attitude, the velocity and the angular velocity. In this paper, the kinematic equations are established according to the coordinate system and the transformation matrix.

$$\dot{\theta}=\omega_y\sin\phi+\omega_z\cos\phi \tag{12}$$

$$\dot{\psi}=\omega_y\sec\theta\cos\phi-\omega_z\sec\theta\sin\phi \tag{13}$$

$$\dot{\phi} = \omega_x - \omega_y \tan\theta\cos\phi + \omega_z \tan\theta\sin\phi \tag{14}$$

$$\dot{x}_0 = v_x \cos\theta\cos\psi + v_y \left(\sin\psi\sin\phi - \sin\theta\cos\psi\cos\phi\right) + v_z \left(\sin\psi\cos\phi - \sin\theta\cos\psi\sin\phi\right) \tag{15}$$

$$\dot{y}_0 = v_x \sin\theta + v_y \cos\theta\cos\phi - v_z \cos\theta\sin\phi \tag{16}$$

$$\dot{z}_0 = -v_x \cos\theta\sin\psi + v_y \left(\cos\psi\sin\phi + \sin\theta\sin\psi\cos\phi\right) + v_z \left(\cos\psi\cos\phi - \sin\theta\sin\psi\sin\phi\right) \tag{17}$$

$$v^2 = v_x^2 + v_y^2 + v_z^2 \tag{18}$$

$$\alpha = -\arctan\left(v_y / v_x\right) \tag{19}$$

$$\beta = \arctan\left(v_z \Big/ \sqrt{v_x^2 + v_y^2}\right) \tag{20}$$

$$\sin\Theta = \sin\theta\cos\alpha\cos\beta - \cos\theta\cos\phi\sin\alpha\cos\beta - \cos\theta\sin\phi\sin\beta \tag{21}$$

$$\begin{aligned} \sin\Psi\cos\Theta = {}& \sin\psi\cos\theta\cos\alpha\cos\beta + \cos\psi\sin\phi\sin\alpha\cos\beta + \\ & \sin\psi\sin\theta\cos\phi\sin\alpha\cos\beta - \cos\psi\cos\phi\sin\beta + \sin\psi\sin\theta\sin\phi\sin\beta \end{aligned} \tag{22}$$

$$\sin\Phi_c \cos\Theta = \sin\theta\cos\alpha\sin\beta - \cos\theta\cos\phi\sin\alpha\sin\beta + \cos\theta\sin\phi\cos\beta \tag{23}$$

Where $\dot{\theta}$, the pitching angular velocity; $\dot{\psi}$, the yaw angular velocity; $\dot{\phi}$, the roll angular velocity; $\dot{x}_0$, $\dot{y}_0$, $\dot{z}_0$, the velocities of the towed body in the ground coordinate system along the direction of *x*, *y*, *z*, respectively.

2.2.5 Munk moment

By solving the above 23 equations, the whole motion parameters of the space motion of the towed body are obtained, in which the Munk moment is applied to the kinetic equation of the towed body in the form of its dimensionless position derivative of the motions state. The forces of the ideal fluid on the towed body are composed of three parts of linear superposition, which are the ideal fluid forces and moments due to the unsteady motion of the towed body, the constant rotation and the steady motion of the towed body.

$$\begin{cases} M_{\alpha ix} = \left(\lambda_{22} - \lambda_{33}\right)v_y v_z - \lambda_{32}v_y^2 + \lambda_{23}v_z^2 + \left(\lambda_{21}v_z - \lambda_{31}v_y\right)v_x \\ M_{\alpha iy} = \left(\lambda_{33} - \lambda_{11}\right)v_z v_x - \lambda_{13}v_z^2 + \lambda_{31}v_x^2 + \left(\lambda_{32}v_x - \lambda_{12}v_z\right)v_y \\ M_{\alpha iz} = \left(\lambda_{11} - \lambda_{22}\right)v_x v_y - \lambda_{21}v_x^2 + \lambda_{12}v_y^2 + \left(\lambda_{13}v_y - \lambda_{23}v_x\right)v_z \end{cases} \tag{24}$$

With the assumption, the Munk moment formula can be expressed as follows:

$$\begin{cases} M_{\alpha ix} = \left(\lambda_{22} - \lambda_{33}\right)v_y v_z \\ M_{\alpha iy} = \left(\lambda_{33} - \lambda_{11}\right)v_z v_x \\ M_{\alpha iz} = \left(\lambda_{11} - \lambda_{22}\right)v_x v_y \end{cases} \tag{25}$$

As the angle of attack $\alpha = -\arctan\dfrac{v_x}{v_y}$, the sideslip angle $\beta = -\arctan\dfrac{v_z}{\sqrt{v_x^2+v_y^2}}$, assuming that the angle of attack and sideslip angle are small, the Munk moment can be rewritten as the following:

$$[M] = \frac{1}{2}v^2 \begin{bmatrix} \sin 2\beta & 0 & 0 \\ 0 & \sin 2\beta & 0 \\ 0 & 0 & \sin 2\alpha \end{bmatrix} \cdot \begin{bmatrix} \lambda_{22} - \lambda_{33} & 0 & 0 \\ 0 & \lambda_{33} - \lambda_{11} & 0 \\ 0 & 0 & \lambda_{11} - \lambda_{22} \end{bmatrix} \tag{26}$$

From the above deduction, the Munk moment is actually proportional to the v^2, $\sin(2\alpha)$ and $\sin(2\beta)$ and λ_{MM}, which is consistent with the expression of the Munk moment $M = \frac{1}{2} \cdot C_{mm} \cdot M \cdot \sin(2\alpha) \cdot v^2$ given in the commercial software OrcaFlex. Here, λ_{MM} is the $M \cdot C_{mm}$, the product of the Munk moment coefficient C_{mm} of the OrcaFlex and the mass of the water currently displaced by the towed body M. Therefore, in this paper, OrcaFlex is used to establish the model of the towed cable-array under different Munk moment coefficients during turning maneuver.

3. Numerical model set-up

The main sea boundary conditions for the system are as following. The depth of the sea is 1500m. The current speed is 0m/s. The vessel speed is 3m/s. The turning angular velocity is 0.45 deg/s. To simplify the numerical model, the total simulation time is 1600s. The towed body is modelled by the 6D buoy. The diameter of the cable is 0.5m. The axial stiffness of the cable EA is 6000KN. The bending stiffness EI is 0. The linear density is 0.0011t/m. To ensure the stability of the towed system, the towed ship will first tow the cable for 450s, so that the towed system can reach the initial balance of its position and speed before turning. Figure 1 depicts the towed cable-array system under Munk moment. The diagram of towed body in OrcaFlex is shown in Figure 2. The modeling in OrcaFlex is realized through mathematical model. Therefore, the complex curvature of the towed body in Figure 1 can only be replaced by a simplified cylinder. The four yellow flaps represent the tail rudders of the towed body, which are used to control the steering of the towed body. The dark blue background represents the sea level, and the brown background represents the seabed. The basic parameters of the towed body are shown in Table. 1 and Table 2.

In order to verify the correctness of the lumped mass method, a towed cable based on the mathematical formulation above is taken [42]. The calculation results are compared with the previous results. The towed cable includes three sections: cable, array, drogue. The properties of the towed cable are shown in Table. 3. The towed cable-array system used for validation is shown in Figure 3. Point A which is located at 8.2 m of the array section is selected to make some comparisons between the lumped mass model and the previous

research. The variations of depth of point A are compared to the results of Gobat [43] and Ablow [44]. Figure. 4 indicates that the results from the lumped mass model are consistent with the previous work. All the comparisons have validated the lumped mass method.
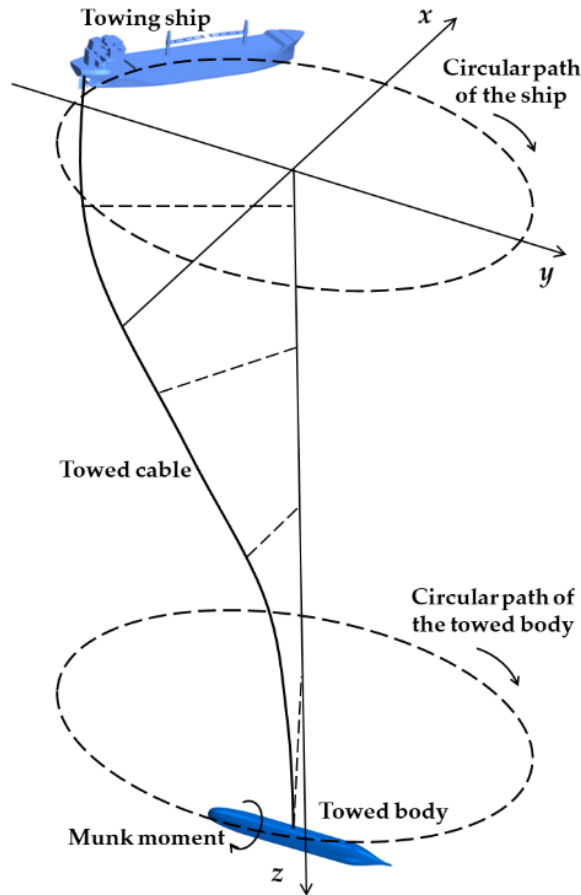

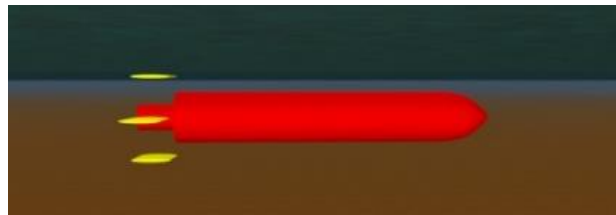**Figure. 1. The towed cable-array system under Munk moment.**

Figure. 2. The diagram of towed body in OrcaFlex.

Table 1. The basic parameters of the towed body.

| Mass(t)	Mass moments of Inertia(t.m²)			Total Length(m)	Centre of Mass(m)		
	I_x	I_y	I_z		x	y	z
1.5	0.1	5	5	3.9	0	0	0

Table 2. The basic parameters of the towed body structure.

| Cylinder segment	Inner diameter (m)	Outer diameter (m)	Length(m)	Cumulative Length(m)
1	0	0.2	0.1	0.1

2	0	0.35	0.3	0.4
3	0	0.5	1.0	1.4
4	0	0.5	1.0	2.4
5	0	0.4	1.0	3.4
6	0	0.2	0.5	3.9

Table 3. Characteristics of towed cable system for validation.

Parameter	Cable	Array	Drogue
Length(m)	723	273.9	30.5
Mass per length(kg/m)	1.5895	5.07	0.58
Wet weight per length(N/m)	2.33	0	0.57
Diameter(m)	0.041	0.079	0.025
Axial stiffness EA(N)	1×10^8	1×10^8	5×10^6
Bending stiffness EI(N.m)	1000	1000	0.01
ρ_w	2	1.8	1.8
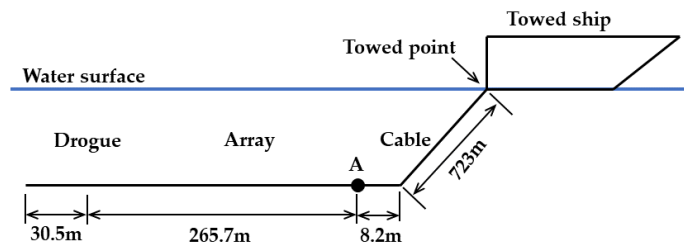
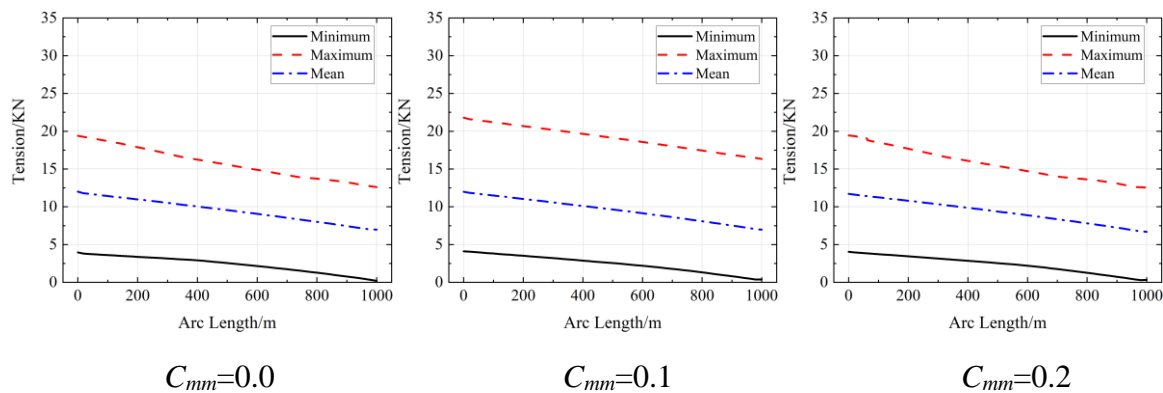**Figure. 3. Validation model for the lumped mass method.**
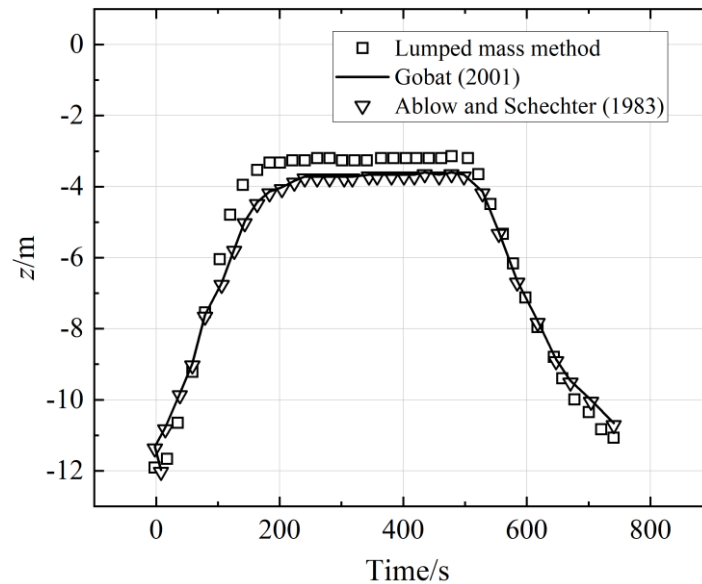
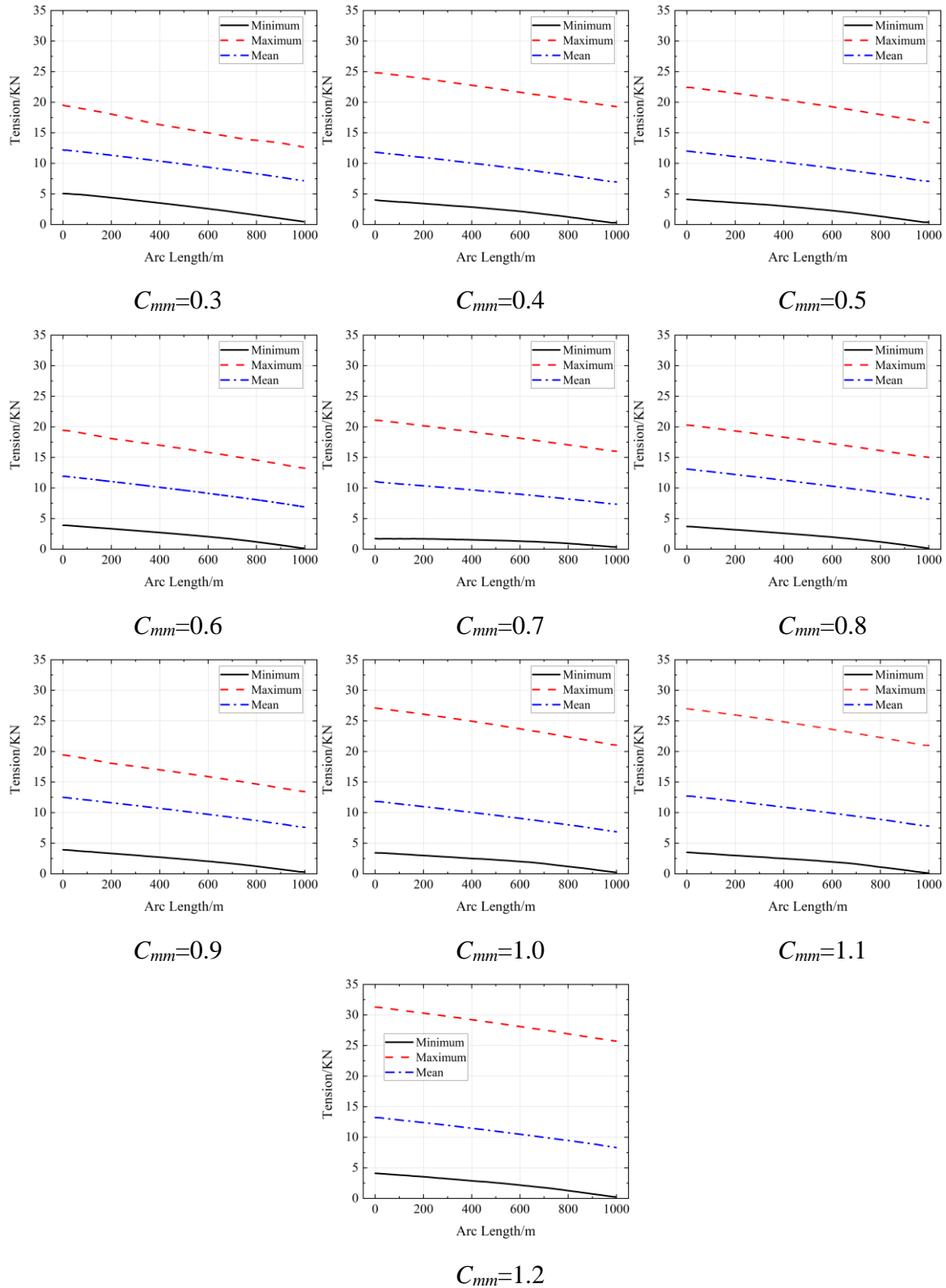**Figure. 4. Validation results for the lumped mass method.**

4. Results and discussion

4.1 The tension of the towed cable under different Munk moment coefficients

Figure 5 shows the cable tension under different Munk moment coefficients from C_{mm}=0 to C_{mm}=1.2. With the increase of Munk moment coefficient, the tension of the towed cable is not always on the increase. When Munk moment coefficient increases from 0 to 0.1, the tension of the towed cable along the length direction increases significantly. When Munk moment coefficient continues to increase to 0.2-0.3, the tension of the towed cable along length direction begin to reduce by small amplitude. When Munk moment coefficient increase to 0.4, the tension along the length direction increases by large amplitude. When Munk moment coefficient increases to 0.4-0.6, the tension along the cable length direction decreases in turn. When Munk moment coefficient increases to 0.7, the tension along the length direction increases again, and when Munk moment coefficient continues to increase to 0.7-0.9, the tension along cable length direction again decreases in turn. When Munk moment coefficient increases to 1, the tension along the length direction increases greatly. When Munk moment coefficient increases to 1-1.2, the tension along the cable length direction does not decrease, but continues increasing in turn.

The reason for this phenomenon is that when Munk moment coefficient is small, the drag force caused by Munk moment makes the underwater towed body rotate. The flow facing surface area change constantly, sometimes large, sometimes small. When it is large, the drag force and the damping force on the towed body of the current would become larger, which makes the towline tension larger. When Munk moment coefficient continues to increase, Munk moment and some other moments on the towed body make the towed body rotate to a certain state, no longer have the rotation. The flow facing surface area also no longer change, thus making this drag force and damping force of water flow do not change, then make the distribution of the tension along the cable length direction to a certain extent, and the tension do not change any more in such a state.
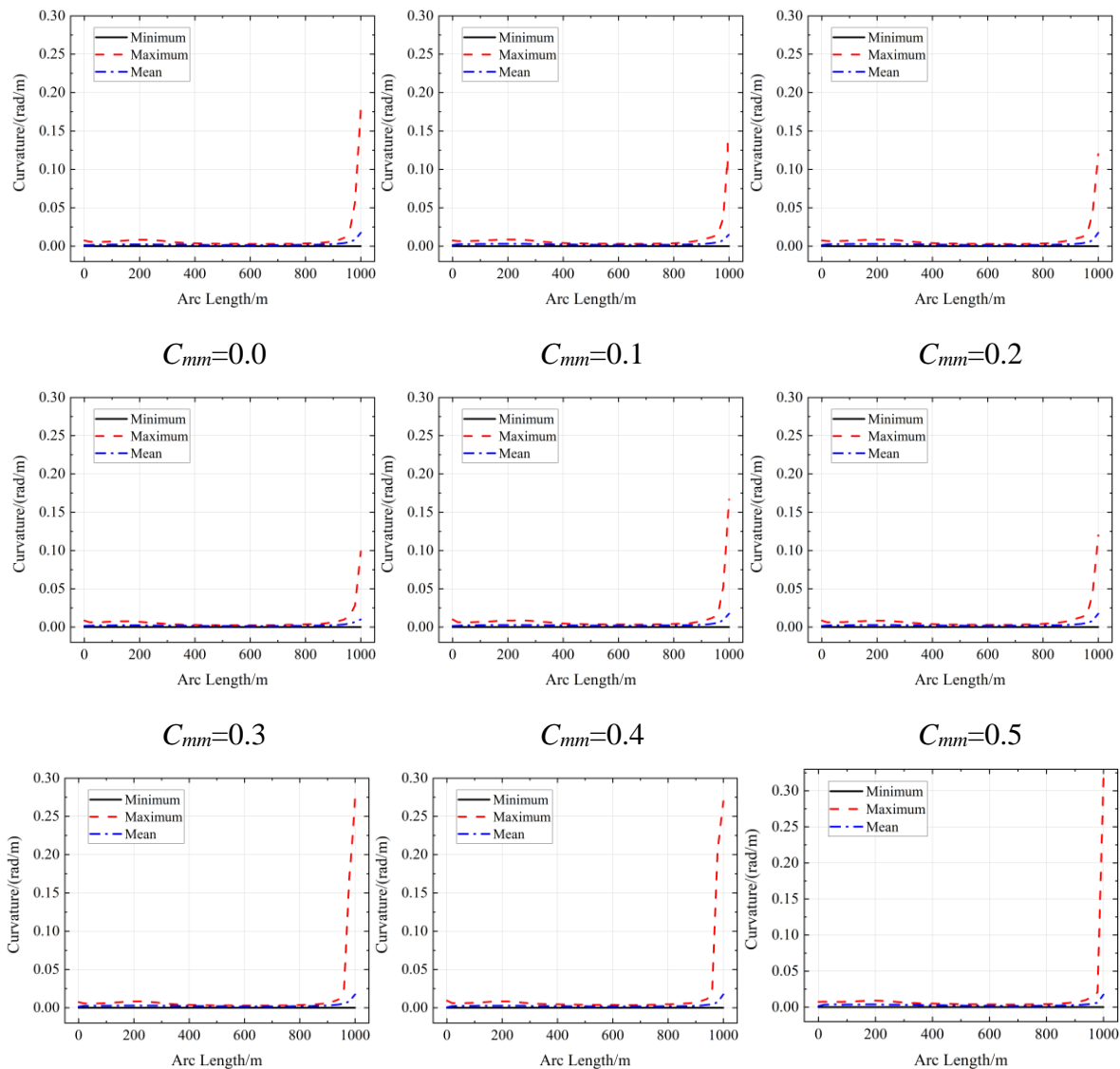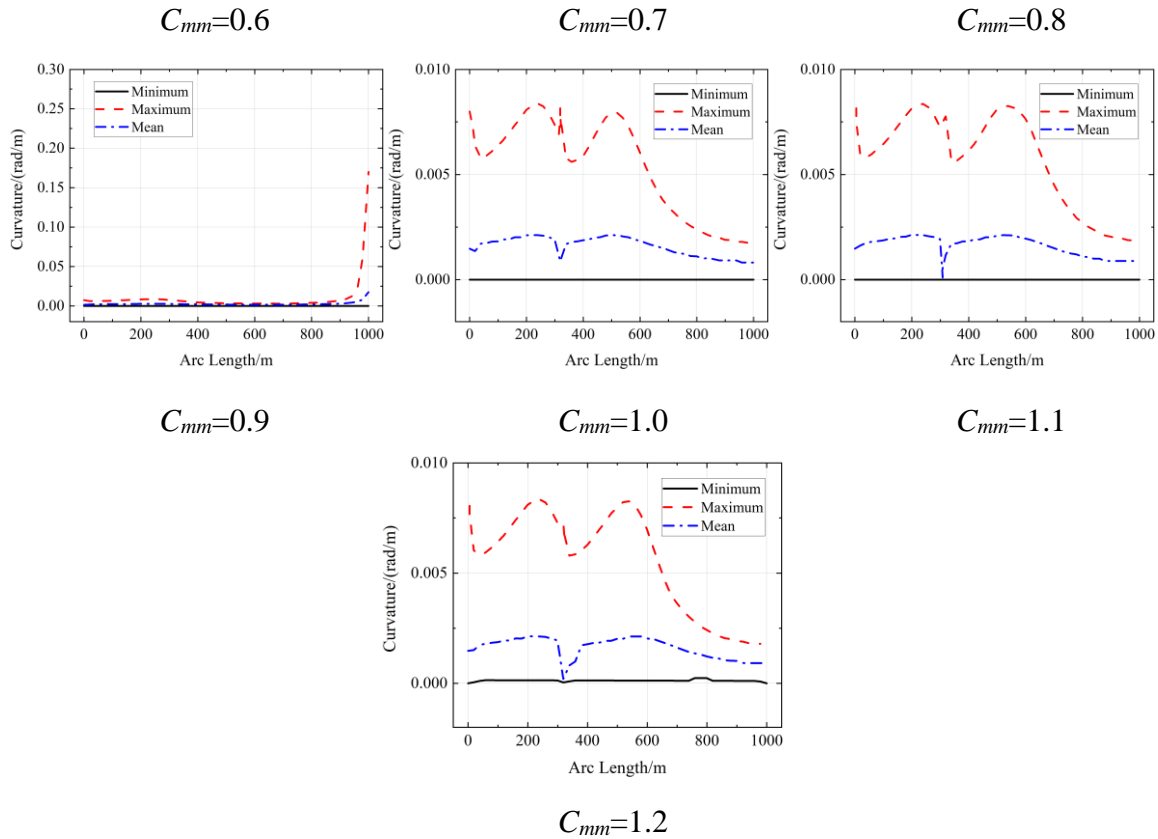

C_{mm}=0.0 C_{mm}=0.1 C_{mm}=0.2

C_{mm}=0.3 C_{mm}=0.4 C_{mm}=0.5

C_{mm}=0.6 C_{mm}=0.7 C_{mm}=0.8

C_{mm}=0.9 C_{mm}=1.0 C_{mm}=1.1

C_{mm}=1.2

Figure. 5. The minimum, maximum and mean tension of the cable under different Munk moment coefficients ranging from 0-1.2.

4.2 The curvature of the towed cable under different Munk moment coefficients

Figure 6 shows the cable curvature under different Munk moment coefficients form $C_{mm}=0$ to $C_{mm}=1.2$. To observe the changes of the curvature along the length direction of the towed cable, it can be found that the curvature doesn't increase with the increasing of Munk moment coefficient. When Munk moment coefficient increases from 0 to 0.9, the curvature of the towed cable is approximately 0 from 0m-800m. The curvature goes up quickly from 800m-1000m, and then the curvature in the vicinity of 1000m rapidly becomes 0. And with Munk moment coefficient increases, the curvature changes with cyclic variation. When Munk moment coefficient are 1-1.2, at the curvature along the towed cable length everywhere are minimal, approximately 0, especially near the towed body. The reason for this phenomenon is that when Munk moment coefficient is small, the resistance of Munk moment causes the towed body to rotate, and the surface area of the water flow surface changes, which leads to the torsion and twining cycle of the cable. If Munk moment coefficient continues to increase to a large value, the large Munk moment makes the towed body have a trend away from the cable, and the cable is straightened and keeps being stretched the straightened state.

$C_{mm}=0.0$

$C_{mm}=0.1$

$C_{mm}=0.2$

$C_{mm}=0.3$

$C_{mm}=0.4$

$C_{mm}=0.5$

C_{mm}=0.6 C_{mm}=0.7 C_{mm}=0.8

C_{mm}=0.9 C_{mm}=1.0 C_{mm}=1.1
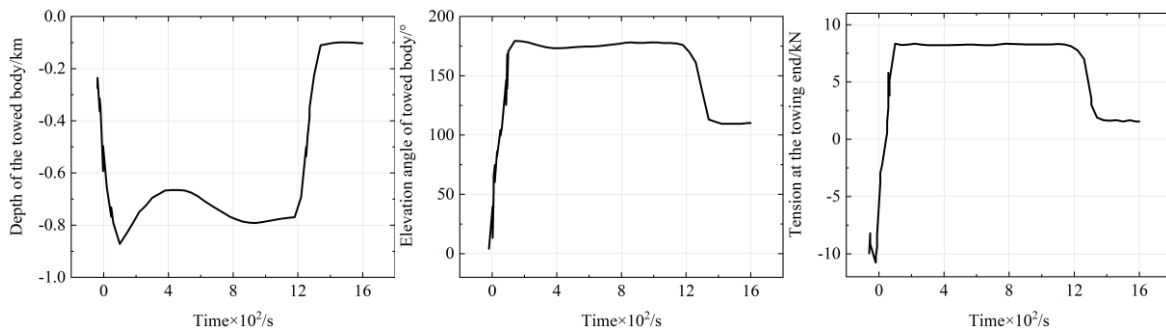
C_{mm}=1.2

Figure. 6. The minimum, maximum and mean curvature of the cable under different Munk moment coefficients ranging from 0-1.2.

4.3 Variety of depth and elevation angle of towed body and tension at the towing end in time domain

Figure 7 depicts the depth and elevation angle of the towed body and tension at the towing end during turning maneuver. Before 1200s, the depth of the towed body drops, which indicates that the towed body is sinking in this stage. Correspondingly, the towing cable is under tension, and the tension at the towing end is maintained at about 8kN. The variety of elevation angle indicates that the whole towed cable-array system is stable. The change of Munk moment has little effect on the attitude of the towed body and the tension at the towing end.

Figure. 7. The minimum, maximum and mean curvature of the cable under different Munk moment coefficients ranging from 0-1.2.

4. Results and discussion

In this paper, a numerical model of a towed cable-array system is established using lumped mass method to study the hydrodynamic characteristic under the Munk moment during turning maneuver. This study demonstrated the following:

(1) The effect of Munk moment on the tension of the towed cable is mainly concentrated on the maximum value. The greater the Monk moment, the greater the maximum value of the cable tension. This means that the ultimate tension on the cable is also greater. Therefore, when the towed body encounters Munk moment, maximum value shall be paid attention to in the design of the cable.

(2) When Munk moment is small, Munk moment makes the towed body rotate, and the area of the upstream surface constantly changes. When the area of the upstream sur-face is larger, the drag force and damping force on the towed body acted by the current are larger, which lead to the larger tension of the towing cable. When Munk moment coefficient continues to increase, under the action of Munk moment and other moments, the towed body first rotates to a certain state and then stops rotating. The area of the upstream surface will not change, so that the drag force and damping force will not change at this time. In this state, the tension distribution along the cable length direction will not change after increasing to a certain extent.

(3) The effect of Munk moment on the curvature of the towed cable is mainly concentrated on the position near the towed body. When Munk moment is small, the curvature along the length direction of the towed cable changes with cyclic variation. When Munk moment is large enough, the curvature along the towed cable length is minimal, approximately 0, especially near the towed body. At this time, the towed body tends to be far away from the cable, and the cable is tensioned and straightened. The space attitude and relative position of the towed body in the water will not change, which means that the shape of the cable at this time will also not change, and it will remain tensioned and straightened.

It should be noted that in order to simplify the calculation model and shorten the calculation time, this paper mainly considers Munk moment suffered by the towed body, but does not consider Munk moment suffered by the cable. In the next step of research, this will be further studied.

References:

1. Han, Y.; Zhou, L.; Ding, S.; Zhang, M.; Guan, Y. Course stability analysis for towing system of a gravity-based structure in managed ice fields. *Ships Offshore Struc* **2021**, 1-13.

2. Andriolo, A.; Castro, F.R.D.; Amorim, T.; Miranda, G.; Tullio, J.D.; Moron, J.; Ribeiro, B.; Ramos, G.; Mendes, R.R. Marine Mammal Bioacustics Using Towed Array Systems in the Western South Atlantic Ocean. In *Advances in Marine Vertebrate Research in Latin America*, Springer: 2018; pp 113-147.

3. Chi, C.; Pallayil, V.; Chitre, M. Design of an adaptive noise canceller for improving performance of an autonomous underwater vehicle-towed linear array. *Ocean Eng* **2020**, 202, 106886.

4. Li, B.; Huang, W.; Liang, H. An efficient method to assess effect of fin on the course stability of towing system. *Ocean Eng* **2020**, 217, 108005.

5. Bettles, R.W.; Chapman, D.A. The experimental verification of a towed body and cable dynamic response theory. *Ocean Eng* **1985**, 12, 453-469.

6. Wu, J.; Chwang, A.T. A hydrodynamic model of a two-part underwater towed system. *Ocean Eng* **2000**, 27, 455-472.

7. Wu, J.; Chwang, A.T. Experimental investigation on a two-part underwater towed system. *Ocean Eng* **2001**, 28, 735-750.

8. Kishore, S.S.; Ganapathy, C. Analytical investigations on loop-manoeuvre of underwater towed cable-array system. *Appl Ocean Res* **1996**, 18, 353-360.

9. Srivastava, S.K.; Ganapathy, C. Experimental investigations on loop manoeuvre of underwater towed cable-array system. *Ocean Eng* **1998**, 25, 85-102.

10. Gobat, J.I.; Grosenbaugh, M.A. Time-domain numerical simulation of ocean cable structures. *Ocean Eng* **2006**, 33, 1373-1400.

11. Holmes, J.D.; Carey, W.M.; Lynch, J.F.; Newhall, A.E.; Kukulya, A. An autonomous underwater vehicle towed array for ocean acoustic measurements and inversions, Europe Oceans: 2005; pp 1058-1061.

12. Grosenbaugh, M.A. Transient behavior of towed cable systems during ship turning maneuvers. *Ocean Eng* **2007**, 34, 1532-1542.

13. Wang, Z.; Sun, G. Parameters influence on maneuvered towed cable system dynamics. *Appl Ocean Res* **2015**, 49, 27-41.

14. Feng, D.K.; Zhao, W.W.; Pei, W.B.; Ma, Y.C. A new method of designing Underwater Towed System, Applied Mechanics and materials, Trans Tech Publ: 2011; pp 1251-1255.

15. Carey, W.M.; Holmes, J.D.; Lynch, J.F. The applicability of a small autonomous vehicle towed array system to ocean acoustic measurements and signal processing, Proceedings of Meetings on Acoustics 155ASA,: 2008; p 70007.

16. Du, X.; Cui, H.; Zhang, Z. A numerical method for analyzing the influence of underwater vehicle flow field on dynamic behavior of towed sonar cable array. *Ocean Eng* **2019**, 175, 163-175.

17. Zhang, J.; Chang, Z.; Lu, G.; Zheng, Z.; Zhang, Z. Analysis of the Dynamic System of Wave Glider with a Towed Body. *J Ocean U China* **2020**, 19, 519-524.

18. Yang, B.; Zhu, K.; Zhu, Y.; Qin, D. Dynamic response of towed line array. *J Hydro, Ser. B* **2013**, 25, 616-619.

19. Yuan, J.; Sun, F.; Tang, G.; Chen, Z.; Zheng, L.; Yang, X. Research on the Motion Track of Ocean Towing System, International Conference of Pioneering Computer Scientists, Engineers and Educators, Springer: 2019; pp 590-609.

20. Holmes, J.D.; Carey, W.M.; Lynch, J.F. Results from an autonomous underwater vehicle towed hydrophone array experiment in Nantucket Sound. *J Acou Society America* **2006**, 120, L15-L21.

21. Srivastava, V.K.; Sanyasiraju, Y.; Tamsir, M. Dynamic behavior of underwater towed cable in linear profile. *Int J Sci Eng Research* **2011**, 2, 1-10.

22. Zhao, Y.; Li, G.; Lian, L. Numerical model of towed cable body system validation from sea trial experimental data. *Ocean Eng* **2021**, 226, 108859.

23. Li, Z.; Erskine, J.; Caro, S.; Chriette, A. Design and control of a variable aerial cable towed system. *Ieee Robot Autom Let* **2020**, 5, 636-643.

24. Wang, F.; Huang, G.; Deng, D. Steady state analysis of towed marine cables. *J Shanghai Jiaotong U (Science)* **2008**, 13, 239-244.

25. Sun, H.; Li, G.; Chen, G. Dynamic model of cable tension and configuration for vessel at anchor. *J Mar Sci Tech-Japan* **2021**, 26, 1144-1152.

26. Zhang, D.; Zhao, B.; Zhu, K. Mechanical characteristics analysis of horizontal lifting of subsea pipeline with different burial depths. *Front Earth Sc-Switz* **2022**, 10, 1011291.

27. Bai, Y.; Zhang, D.; Zhu, K.; Zhang, T. Dynamic analysis of umbilical cable under interference with riser. *Ships Offshore Struc* **2018**, 13, 809-821.

28. Zhang, D.; Bai, Y.; Soares, C.G. Dynamic analysis of an array of semi-rigid "sea station" fish cages subjected to waves. *Aquacult Eng* **2021**, 94, 102172.

29. Zhang, D.; Bai, Y.; Zhao, W.; Zhu, K. Dynamic analysis of submarine cable during the process of laying back to the seabed. *Ships Offshore Struc* **2020**, 15, 153-161.

30. Da Silva Gomes, S.; Gomes, S.C.P. A new dynamic model of towing cables. *Ocean Eng* **2021**, 220, 107653.

31. Guo, L.; Yuan, Y.; Tang, W.; Xue, H. A numerical investigation on quasi-static configuration and nonlinear dynamic response characteristics of marine towing cable. *Ocean Eng* **2021**, 240, 110007.

32. Westin, C.; Irani, R.A. Modeling dynamic cable-sheave contact and detachment during towing operations. *Mar Struct* **2021**, 77, 102960.

33. Chen, X.; Hong, B.; Lin, Z.; Hou, J.; Gao, Z.; Lv, S. Lumped Mass Model for Flexible Cable: A

Review, Journal of Physics: Conference Series, IOP Publishing: 2021; p 12029.

34. Anderson, J.M.; Chhabra, N.K. Maneuvering and stability performance of a robotic tuna. *Integr Comp Biol* **2002**, 42, 118-126.

35. Tyagi, A.; Sen, D. Calculation of transverse hydrodynamic coefficients using computational fluid dynamic approach. *Ocean Eng* **2006**, 33, 798-809.

36. Hakamifard, M.; Rostami VF, M. Numerical and Analytical Calculation of Munk Moment in Real Flow for an Autonomous Submarine in Pure Sway Motion in PMM Test. *J Solid Fluid Mech* **2019**, 9, 205-216.

37. Hasanloo, D.; Pang, H.; Yu, G. On the estimation of the falling velocity and drag coefficient of torpedo anchor during acceleration. *Ocean Eng* **2012**, 42, 135-146.

38. Orcina. OrcaFlex manual **2015**. http://www.orcina.com/SoftwareProducts/OrcaFlex/Validation/index/.pdf

39. Luo, Y.; Zhang, D. Dynamic analysis of an axially moving underwater pipe conveying pulsating fluid. *Front Mar Sci* **2022**, 9: 982374.

40. Zhang, D.; Zhao, B.; Zhu, K. Hydrodynamic Response of Ocean-Towed Cable-Array System under Different Munk Moment Coefficients. *Sustainability* **2022**, 14, 1932.

41. Sen, D. A study on sensitivity of maneuverability performance on the hydrodynamic coefficients for submerged bodies. *J Ship Res* **2000**, 44, 186-196.

42. Zhu, K.; Zhu, H.; Zhang, Y.; Jie, G.; Miao, G. A multi-body space-coupled motion simulation for a deep-sea tethered remotely operated vehicle. *J Hydro, Ser. B* **2008**, 20, 210-215.

43. Gobat, J.I.; Grosenbaugh, M.A. Dynamics in the touchdown region of catenary moorings. *Int J Offshore Polar* **2001**, 11(4).

44. Ablow, C.M.; Schechter, S. Numerical simulation of undersea cable dynamics. *Ocean Eng* **1983**, 10, 443-457.